*J. Plasma Phys.* (2018), *vol.* 84, 905840308  
doi:10.1017/S0022377818000491

# Molecular dynamics calculation of the spectral densities of plasma fluctuations

**A. Panarese[1,2], D. Bruno[2,†], P. Tolias[3,4], S. Ratynskaia[3], S. Longo[1,2] and U. de Angelis[4]**

[1]Department of Chemistry, University of Bari, Bari 70126, Italy

[2]Institute of Nanotechnology (NANOTEC), CNR, Bari 70126, Italy

[3]Space and Plasma Physics, Royal Institute of Technology (KTH), Stockholm 10044, Sweden

[4]Istituto Nazionale di Fisica Nucleare (INFN), Sezione di Napoli, Naples 80126, Italy

(Received 23 October 2017; revised 4 May 2018; accepted 4 May 2018)

Spectral densities of plasma fluctuations are calculated for the thermal case using classical molecular dynamics (MD) assuming Coulomb interactions and a short-range cutoff radius. The aim of the calculation is to verify limits and performances of such calculations in the light of possible generalizations, e.g. collisional or non-ideal plasmas. Results are presented for ideal, collisionless, fully ionized thermal plasmas. Comparison with the analytical theory reveals a generally satisfactory agreement with possibility for improvement when more strict numerical parameters are used albeit with a strong increase in computational cost. The largest deviations have been observed in the vicinity of the weakly damped eigenmodes. The agreement is strong in other parts of the spectrum, where Landau damping is prominent, and overcomes the effects stemming from the excess collisionality and coupling as well as from the exclusion of short-range collisions.

**Key words:** plasma properties, plasma simulation

## 1. Introduction

The theory of fluctuations constitutes a powerful and versatile formalism that provides a self-consistent description of collisionless fully ionized ideal plasmas (Klimontovich 1967; Akhiezer *et al.* 1975) and is still an active field of research (Schlickeiser 2012; Yoon, Schlickeiser & Kolberg 2014; Kolberg, Schlickeiser & Yoon 2017; Yoon & Lopez 2017). It is based on two fundamental assumptions that concern the omission of high-order fluctuations and the constancy of ensemble averaged quantities in spatio-temporal scales characteristic of the first-order fluctuations (Klimontovich 1967). These assumptions are well justified only in the ideal collisionless case, but fluctuation theory can be adapted for non-ideal plasma systems by invoking a number of additional approximations, e.g. for collisional plasmas, plasma–molecular systems and weakly coupled dusty plasmas (Sitenko & Gurin 1966; Klimontovich *et al.* 1989; Tsytovich & de Angelis 1999; Tolias, Ratynskaia &

†Email address for correspondence: domenico.bruno@cnr.it

de Angelis 2011, 2012). However, in most cases, the validity domain of these extra approximations cannot be rigorously justified, which brings forth the necessity to assess the fluctuation theory results for non-ideal plasmas through simulations. The high number densities and the long-range nature of the electromagnetic force make it computationally prohibitive to perform molecular dynamics (MD) of the real system.

Particle-in-cell (PIC) and Vlasov approaches are efficient ways to simulate collisionless electrostatic (Abdul & Mace 2015; Meierbachtol *et al.* 2017) and electrodynamic plasmas (Lopez & Yoon 2017), respectively. By construction, however, they cannot be used for the simulation of non-ideal plasmas where the role of collisions becomes non-negligible. When collisionality in the plasma cannot be neglected, Ewald summation methods have been proposed (Donko, Kalman & Hartmann 2008; Dharuman *et al.* 2017). For strongly coupled plasmas, like dusty plasmas, pure particle–particle approaches become competitive (see e.g. (Dharuman *et al.* 2017), where they are called linked-cell list (LCL) methods).

Here, we show the performance and limitations of the weighted particle MD (WP-MD) approach. Particle weighting is implemented in a way that preserves the collective properties of the real system. However, the collisional properties of the system are re-scaled, which should influence the spectral densities of fluctuating quantities. This effect can be expected to strongly depend on the probed wavenumber. In this work, we shall validate the algorithm for the calculation of the spectral densities of electron density fluctuations in ideal collisionless non-relativistic electron–proton plasmas. The existence of established analytical formulas for the spectral densities of such a system (Klimontovich 1967; Akhiezer *et al.* 1975; Sheffield 1975; Alexandrov, Bogdankevich & Rukhadze 1984) allows us to investigate the effectiveness of the WP-MD algorithm for different wavenumbers. Although this approach will be much more computationally demanding than a PIC simulation for collisionless plasmas, it will allow us to assess whether it can be confidently employed for non-ideal cases where no rigorous results are available.

## 2. Theory

Electrostatic units are utilized, the temperatures are provided in energy units. The following notations are employed; $\alpha = \{e, i\}$ for the plasma species, $e$ for the elementary charge, $(q_\alpha, m_\alpha, n_\alpha, T_\alpha)$ for the charge, mass, number density and temperature, $v_{\mathrm{T}\alpha} = \sqrt{T_\alpha/m_\alpha}$ for the thermal velocities, $\omega_{\mathrm{p}\alpha} = \sqrt{(4\pi q_\alpha^2 n_\alpha)/m_\alpha}$ for the species plasma frequencies, $\lambda_{\mathrm{D}\alpha} = \sqrt{T_\alpha/(4\pi q_\alpha^2 n_\alpha)}$ for the species Debye lengths and $\lambda_{\mathrm{D}}$ for the plasma Debye length defined by $1/\lambda_{\mathrm{D}}^2 = 1/\lambda_{\mathrm{De}}^2 + 1/\lambda_{\mathrm{Di}}^2$.

In homogeneous weakly coupled plasmas, plasma density fluctuations are fully described by the two-point space–time correlation function defined by $C^\alpha_{\boldsymbol{r},\boldsymbol{r}',t,t'} = \langle \delta n^\alpha_{\boldsymbol{r},t} \delta n^\alpha_{\boldsymbol{r}',t'} \rangle$, where the brackets $\langle \cdots \rangle$ denote the ensemble average over the different realizations of the system, which reduces to $C^\alpha_{\boldsymbol{r},t} = \langle \delta n^\alpha_{\boldsymbol{r},t} \delta n^\alpha_{\boldsymbol{0},0} \rangle$ due to the spatio-temporal translation symmetry (Klimontovich 1967; Akhiezer *et al.* 1975; Alexandrov *et al.* 1984). Unless the heuristic non-interacting limit is considered (Akhiezer *et al.* 1975; Alexandrov *et al.* 1984; Tolias *et al.* 2015), there are no analytic expressions for $C^\alpha_{\boldsymbol{r},t}$. However, convenient closed form relations exist for its space–time Fourier transform $S^\alpha_{\boldsymbol{k},\omega} = \langle |\delta n^\alpha_{\boldsymbol{k},\omega}|^2 \rangle$, typically coined as the spectral density of the plasma density fluctuations. For collisionless non-relativistic fully ionized multi-component plasmas in the absence of external electromagnetic fields, the spectral density of the electron density fluctuations has the general form (Sheffield 1975)

$$S^{\mathrm{e}}_{\boldsymbol{k},\omega} = \left|1 - \frac{\chi^{\mathrm{e}}_{\boldsymbol{k},\omega}}{\epsilon_{\boldsymbol{k},\omega}}\right|^2 S^{\mathrm{e},(0)}_{\boldsymbol{k},\omega} + \left|\frac{\chi^{\mathrm{e}}_{\boldsymbol{k},\omega}}{\epsilon_{\boldsymbol{k},\omega}}\right|^2 \sum_{\alpha\neq\mathrm{e}} \frac{q_\alpha^2}{e^2} S^{\alpha,(0)}_{\boldsymbol{k},\omega}, \tag{2.1}$$

where $\epsilon_{\boldsymbol{k},\omega} = 1 + \sum_\alpha \chi^\alpha_{\boldsymbol{k},\omega}$ is the plasma dielectric permittivity, $\chi^\alpha_{\boldsymbol{k},\omega}$ are the plasma species susceptibilities and $S^{\alpha,(0)}_{\boldsymbol{k},\omega}$ are the spectral densities of the natural plasma density fluctuations. The latter two quantities are given by

$$\begin{aligned}\chi^\alpha_{\boldsymbol{k},\omega} &= \frac{4\pi q_\alpha^2}{m_\alpha k^2} \int \frac{1}{\omega - \boldsymbol{k}\cdot\boldsymbol{v} + \imath 0} \left[\boldsymbol{k}\cdot\frac{\partial \Phi_\alpha(\boldsymbol{v})}{\partial \boldsymbol{v}}\right] \mathrm{d}^3 v \\ &= \frac{1}{k^2\lambda_{\mathrm{D}\alpha}^2}\left[1 + \zeta_\alpha \mathrm{e}^{-\zeta_\alpha^2}\left(\imath\sqrt{\pi} - 2\int_0^{\zeta_\alpha} \mathrm{e}^{t^2}\,\mathrm{d}t\right)\right], \end{aligned} \tag{2.2}$$

$$S^{\alpha,(0)}_{\boldsymbol{k},\omega} = \frac{1}{(2\pi)^3}\int \delta(\omega - \boldsymbol{k}\cdot\boldsymbol{v})\Phi_\alpha(\boldsymbol{v})\,\mathrm{d}^3 v = \frac{1}{(2\pi)^{7/2}}\frac{n_\alpha}{k v_{\mathrm{T}\alpha}}\mathrm{e}^{-\zeta_\alpha^2}, \tag{2.3}$$

with $\zeta_\alpha = \omega/(\sqrt{2}kv_{\mathrm{T}\alpha})$. The first equality is valid for an arbitrary distribution function, whereas the second equality is valid for a Maxwellian distribution function $\Phi_\alpha(\boldsymbol{v}) = n_\alpha[m_\alpha/(2\pi T_\alpha)]^{3/2}\exp\left[-m_\alpha v^2/(2T_\alpha)\right]$. It is apparent from (2.1) that $S^{\mathrm{e}}_{\boldsymbol{k},\omega}$ will have maxima at $\epsilon_{\boldsymbol{k},\omega} \simeq 0$, which correspond to the weakly damped eigenmodes of the system.

Let us consider a thermal plasma consisting of electrons and a singly positively charged ion species; $n_{\mathrm{e}} = n_{\mathrm{i}} = n$, $T_{\mathrm{e}} = T_{\mathrm{i}} = T$ and $m_{\mathrm{i}} \gg m_{\mathrm{e}}$. We focus on the high frequency regime, $\omega \gg kv_{\mathrm{Te}}$, since in this range Langmuir waves propagate, which constitute the only weakly damped mode of the particular system. In the limit of negligible Landau damping $k\lambda_{\mathrm{De}} \ll 1$, it can be proven that $S^{\mathrm{e}}_{\boldsymbol{k},\omega} \to [1/(2\pi)^4]\pi n k^2 \lambda_{\mathrm{De}}^2 \delta(\omega - \sqrt{\omega_{\mathrm{pe}}^2 + 3k^2 v_{\mathrm{Te}}^2})$, see Tolias & Ratynskaia (2013) for the methodology. Therefore, when $k\lambda_{\mathrm{De}} \ll 1$, the electron spectral density for constant wavenumbers behaves as a delta function located at the Langmuir eigen-frequencies. As the wavenumber increases, there is a Lorentzian broadening of the Langmuir peak due to collisionless damping. For high wavenumbers, the peak keeps broadening until it is completely smoothed out, see also figure 1. It is important to emphasize that the Langmuir peak is a local but not necessarily a global maximum.

For thermal plasmas, the electron structure factor $S^{\mathrm{e}}_{\boldsymbol{k}} = \int_{-\infty}^{+\infty} S^{\mathrm{e}}_{\boldsymbol{k},\omega}\,\mathrm{d}\omega$ can be analytically calculated. This quantity is also the Fourier transform of the spatial correlation function of electron density fluctuations $C^{\mathrm{e}}_{\boldsymbol{r}} = \langle \delta n_{\mathrm{e}}^2 \rangle_{\boldsymbol{r}}$ and is the most natural choice for the normalization of $S^{\mathrm{e}}_{\boldsymbol{k},\omega}$. In particular, equation (2.1) can be rewritten as $S^{\mathrm{e}}_{\boldsymbol{k},\omega} \propto \mathrm{Im}\{R_{\boldsymbol{k},\omega}\}/\omega$ where $R_{\boldsymbol{k},\omega}$ is a system response function. Such an expression allows the calculation of $S^{\mathrm{e}}_{\boldsymbol{k}}$ with the aid of the Kramers–Kronig relations. The result reads as (Akhiezer *et al.* 1975)

$$S^{\mathrm{e}}_{\boldsymbol{k}} = \frac{n}{(2\pi)^3}\frac{\frac{1}{2} + k^2\lambda_{\mathrm{D}}^2}{1 + k^2\lambda_{\mathrm{D}}^2}. \tag{2.4}$$

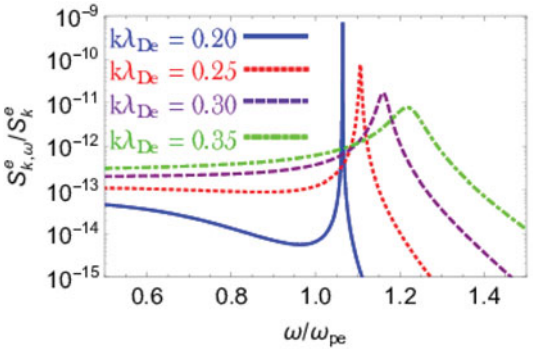


FIGURE 1. The frequency dependence of the normalized spectral density of electron density fluctuations near the Langmuir resonance for varying wavenumbers. Theoretical results from (2.1). As $k\lambda_{De}$ increases, the resonance broadens, the height of the peak decreases and the position of the peak shifts towards higher frequencies as dictated by the Langmuir dispersion relation $\omega^2 = \omega_{pe}^2(1 + 3k^2\lambda_{De}^2)$.

## 3. Numerical method

The numerical method employed in this work for the calculation of the space–time correlation function of electron density fluctuations is based on molecular dynamics in the $(\boldsymbol{r}, \boldsymbol{v})$ space using an importance sampling Monte Carlo (Tolias *et al.* 2015). In contrast to Tolias *et al.* (2015) that focused on the non-interacting electron gas and the spectral densities of natural electron density fluctuations, here interactions are included. In the non-relativistic limit $|\boldsymbol{v}| \ll c$, magnetic field generation and retardation effects are negligible. Hence, it suffices to consider only electrostatic interactions as Coulomb forces between all particle pairs. The simulation is mesh free and there is no discretization in the $(\boldsymbol{r}, \boldsymbol{v})$ space.

*The particle weight.* Due to the high computational cost, the simulated particle density is much smaller than in the real system. Each simulated particle corresponds to a cluster of real particles. Denoting the simulation quantities with the superscript $s$, the particle weight or scaling factor is defined by $n = wn^s$ or equivalently by $w = (n/N^s)V$ with $V$ the simulation volume. In order to ensure that quantities which characterize collective plasma properties (Debye lengths, plasma frequencies, thermal velocities) are equal to those in the real system, the following scalings are applied to the electric charges, particle masses and species temperatures: $e^s = we$, $m_\alpha^s = wm_\alpha$, $T^s = wT$. However, the above scalings imply that quantities which characterize collisional plasma properties such as the average electron–ion collision frequency $\bar{\nu}_{ei} \propto (ne^4)/(\sqrt{m_e}T^{3/2})$, the Coulomb radius $r_C \propto e^2/T$ and the unscreened coupling parameter $\Gamma \propto e^2/(n^{-1/3}T)$ differ from those in the real system. In particular, we have $\bar{\nu}_{ei}^s = w\bar{\nu}_{ei}$, $r_C^s = wr_C$ and $\Gamma^s = w^{2/3}\Gamma$. As we shall see, these effects (collisionality, large angle scattering, strong coupling) will lead to deviations from the theory.

*The numerical equations of motion.* The Newton equations are integrated for all simulated particles in discrete time steps with the velocity Verlet algorithm. The simulated system's equations of motion differ from the real system's equations of motion not only due to the introduction of the particle weight $w$ but also due to the necessity of tackling some issues caused by the discrete time step. (i) The finiteness of the integration time step introduces errors in the particle trajectories. Small errors in the particle positions can cause large errors in the particle velocities in the case of

very close encounters. Particles could end up lying at mutual distances much shorter than energetically permitted, an effective source of energy that must be kept under control. We choose a simple scheme to tackle this problem, by neglecting interactions among particles at distances shorter than a fixed cutoff radius $r_0$. Clearly, shorter time steps allow us to decrease the value of this numerical parameter. However, decreasing it below the simulated Coulomb radius has the adverse effect of permitting the inclusion of spurious large angle collisions. A detailed discussion on the optimal choice of this parameter is provided in § 5. (ii) Even with the introduction of $r_0$, the discreteness of the integration time step still prevents the exact conservation of the total energy. In the long run, this leads to an increase of the total energy of the system. Consequently, the temperature of the simulated system does not fluctuate around its prescribed value, but slowly increases with time. The temperature is kept constant in the simulation by implementing a Nosé thermostat (Nosé 1984), i.e. by subjecting each particle to a frictional force $\propto \boldsymbol{v}_i$. The efficiency of the thermostat is controlled via the simulation parameter $\eta$, the value of the numerical viscosity should be large enough to maintain the prescribed average temperature and small enough to ensure that the additional dissipation does not significantly perturb the dynamics. Given the above, each simulated particle is subject to the following force:

$$\boldsymbol{F}_i = -\sum_{j\neq i} \nabla\phi_{ij} - \eta\frac{T-T_0}{T_0}\boldsymbol{v}_i \tag{3.1}$$

$$\phi_{ij} = w^2 q_i q_j \times \begin{cases} \dfrac{1}{|\boldsymbol{r}_i - \boldsymbol{r}_j|}, & |\boldsymbol{r}_i - \boldsymbol{r}_j| > r_0, \\ \dfrac{1}{r_0}, & |\boldsymbol{r}_i - \boldsymbol{r}_j| \leqslant r_0, \end{cases} \tag{3.2}$$

where $T$ and $T_0$ are the instantaneous and the prescribed equilibrium temperatures, respectively.

*The boundary conditions.* Periodic boundary conditions are implemented as follows: (i) Concerning the particle motion, each simulated particle behaves as if the simulation volume was periodic along all three dimensions. (ii) Concerning the forces, each simulated particle feels the presence of all other simulated particles and of the periodic images of all particles (including itself) along the three dimensions, up to the nearest neighbour, i.e. 26 images.

*The spectral density of fluctuations.* In the simulation, the fluctuations of the electron number density $\delta n_\mathrm{e}(\boldsymbol{r}, t) = n_\mathrm{e}(\boldsymbol{r}, t) - n_0$ are sampled at discrete times on a spatial grid. For an isotropic system, it is sufficient to sample on a one-dimensional spatial grid. It is worth underlining that the spatial mesh used for the sampling does not affect the system dynamics. The sampled signal is then doubly Fourier transformed in space and time using standard fast Fourier transform (FFT) routines (Frigo & Johnson 2005) and squared to get the fluctuation power spectrum. The particle weight $w$ and the sampling on a discrete mesh introduce a scaling factor so that the power spectrum from the simulation is related to that in the real system by

$$S^\mathrm{e}_{\boldsymbol{k},\omega} = w\frac{\Delta t}{N_\mathrm{t}}\frac{1}{V}S^\mathrm{s}_\mathrm{e}(k, \omega), \tag{3.3}$$

where $\Delta t$ is the interval between two successive samplings, $N_\mathrm{t}$ is the number of sampled points in time and $V$ is the volume of the simulation box. The spectra are

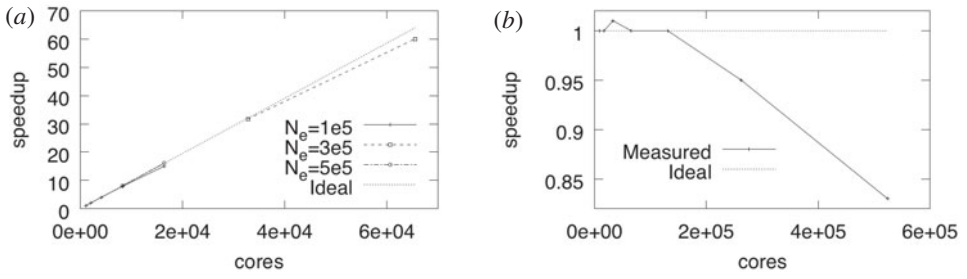


FIGURE 2. Scaling properties. (*a*) Strong scaling for different problem sizes. (*b*) Weak scaling with fixed load per node.

then normalized by the theoretical electron structure factor, equation (2.4). Finally, spectra obtained from multiple independent runs are averaged in order to reduce the statistical scatter. Such ensemble averaging also allows us to estimate the variance of the results.

## 4. Algorithm and scalability

The computational cost is driven by the force calculations which scale as $\sim(N^s)^2$. As a consequence, the running time scales linearly with the number of time steps and quadratically with the number of simulated particles. The basic algorithm has been adapted to run on multi-node hardware with message passing interface (MPI) parallelization. The total number of particles is divided evenly among the MPI ranks. Each MPI rank has its own cores perform the operations on its designated chunk of particles, with the following modifications: (i) A global list of particle positions is updated after the movement step via an ALLGATHER operation. (ii) The forces acting on the particles local to the MPI rank are calculated by taking into account the influence of all particles via the global list above.

Scalability tests have been run for a small number of time steps. The code has demonstrated excellent scaling properties for the simulation parameters of interest. Figure 2(*a*) shows a strong scaling curve obtained on Fermi (CINECA, Italy) for different problem sizes. The scalability is excellent up to 65 536 cores (4096 nodes) and the parallel efficiency is always better than 95 %. Figure 2(*b*) reports the results for a weak scaling curve obtained on JuQueen (FZJ, Germany). This time the number of particles is chosen such that the load per node is constant, i.e. we have set $(N_e^s)^2/N_n = 10^7$, where $N_n$ is the number of nodes (each node has 64 cores). The code again shows very good scaling capabilities. Some performance degradation can only be seen at the largest number of cores where a good parallel efficiency can be recovered with larger problem sizes (not shown here). Production runs have been carried out on Galileo (CINECA, Italy), exploiting the availability of accelerators (Intel Xeon Phi) by offloading part of the force calculation routine, which is the bottleneck of the simulation. A typical run with $N_e^s = 25\,000$ and 9000 time steps takes 15.5 hours on 4 nodes (each node has 16 cores and 2 accelerators). Except where otherwise stated, the spectra shown here have been obtained by ensemble averaging over typically 50 independent runs.

## 5. Model problem and implementation

The choice of the plasma parameters is based on restricting to fully ionized and collisionless plasmas – hence dense and hot plasmas to ensure we deal with

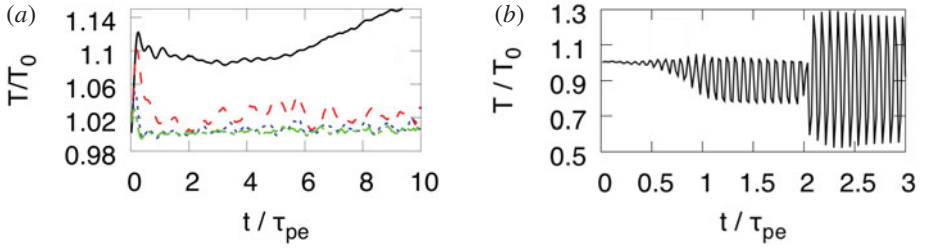


FIGURE 3. Time evolution of the electron temperature for different values of the viscosity. (*a*) Black: $\eta = 10^{-20}$, red: $\eta = 10^{-19}$, blue: $\eta = 5 \times 10^{-19}$, green: $\eta = 10^{-18}$; (*b*) $\eta = 5 \times 10^{-18}$.

an ideal plasma scenario. The wavenumbers are selected to reflect cases ranging from undamped Langmuir resonances to Landau damped broadened features of the spectral density of the electron density fluctuations. We thus simulate a thermal plasma consisting of electrons and protons, with the density of $n = 10^{20}$ m$^{-3}$ and the temperature of $T = 1$ keV. The real and simulated systems have the following values for the characteristic collective parameters: $\lambda_{De} = \lambda_{Di} = 2.35 \times 10^{-5}$ m, $\omega_{pe} = 5.6 \times 10^{11}$ rad s$^{-1}$ and $\omega_{pi} = 1.3 \times 10^{10}$ rad s$^{-1}$, while the real system has the following values for the characteristic collisional parameters: $r_C = 1.44 \times 10^{-12}$ m, $\Gamma = 10^{-5}$ and $\bar{\nu}_{ei} = 1.5 \times 10^5$ s$^{-1}$. The smallest wavenumber investigated in this work is $k = 10^4$ m$^{-1}$ and corresponds to $k\lambda_{De} = 0.235$. The simulation domain, unless stated otherwise, is a cubic box of dimension $L = 2\pi \times 10^{-4}$ m $= 26.73\ \lambda_{De}$.

*The numerical viscosity*. As mentioned, a thermostat has been introduced in order to prevent a rise in the temperature of the simulated system. We therefore investigated the impact of this artificial viscosity on the simulation results. Figure 3(*a*,*b*) illustrates the temporal profiles of the system temperature for $N_e^s = 5000$ and different values of the numerical viscosity $\eta$ that governs the thermostat efficiency. Apart from an initial transient, the system exhibits a steady behaviour. Small values of $\eta$ result to a system temperature deviating from the prescribed temperature – see the black line in figure 3(*a*), whereas large values of $\eta$ essentially drive the particle dynamics – see figure 3(*b*). In this latter case, also the resulting spectrum is affected, as demonstrated in figure 4(*a*). We have drawn the conclusion that the value $\eta = 10^{-19}$ gives the best compromise for our model problem. Hence, this value is employed in all the simulations that follow.

*The boundary conditions*. In order to assess the impact of the adopted boundary conditions, the charge distribution in the simulations has been investigated. For an ideal plasma, the electrostatic potential around an elementary point charge is $\phi(r) = (e/r)\ \exp\ (-r/\lambda_D)$. Within the linearized Boltzmann relation, the stationary ion and electron densities around this test charge will be $n_i(r) = n[1 - e\phi(r)/T]$ and $n_e(r) = n[1 + e\phi(r)/T]$, respectively. This results in a net charge profile

$$q(r)/e = 4\pi \int_0^r x^2 [n_i(x) - n_e(x)]\, dx = -1 + \left(1 + \frac{r}{\lambda_D}\right) e^{-r/\lambda_D}. \tag{5.1}$$

Figure 5 shows results on the average net charge around a positive test charge as obtained in simulations with $N_e^s = 5000$, $r_0 = 1.0\ \lambda_{De}$ or $r_0 = 0.1\ \lambda_{De}$. Simulation results are compared to the theoretical result, equation (5.1). We conclude that the agreement

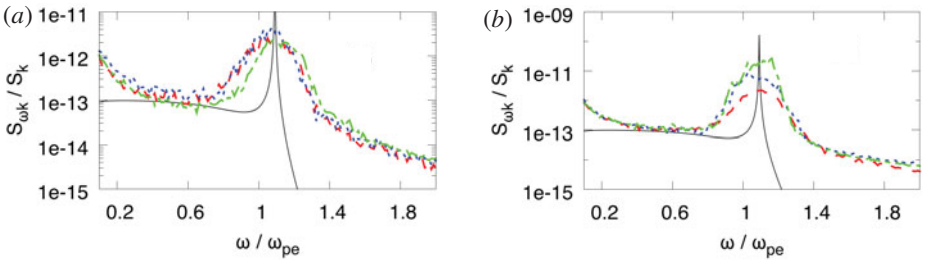


FIGURE 4. Spectral densities of electron density fluctuations for $k = 10^4$ m$^{-1}$, $r_0 = 1.0\ \lambda_{De}$. (*a*) Dependence on the value of the viscosity. Black: theory, red: $\eta = 10^{-20}$, blue: $\eta = 10^{-19}$, green: $\eta = 5 \times 10^{-18}$. (*b*) Dependence on the number of simulated particles. Black: theory, red: $N_e^s = 5000$, blue: $N_e^s = 25\,000$, green: $N_e^s = 75\,000$.

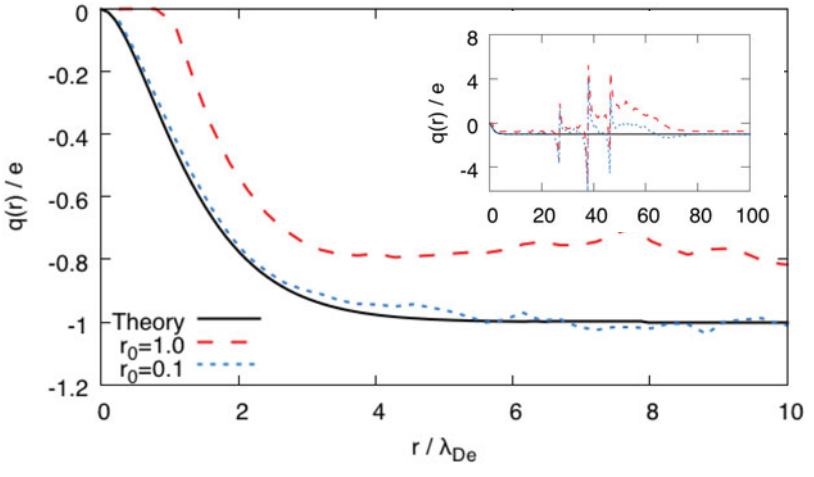


FIGURE 5. Net charge cumulative distribution around a positive test charge: comparison of the $r_0 = 1.0\ \lambda_{De}$ and $r_0 = 0.1\ \lambda_{De}$ cases with the theoretical result for $N_e^s = 5000$. The simulation box is a cube of dimension $L = 26.73\ \lambda_{De}$.

is very good already for $r_0 \leqslant 0.1\ \lambda_{De}$. The periodic boundary conditions introduce a discontinuous behaviour in the charge distribution at distances corresponding to the simulation box dimensions – see the inset of figure 5, but this does not affect the fluctuation spectra at the shorter wavelengths, as we shall see in what follows.

*The simulation duration*. It is important to discern the minimum value for the simulation duration that suffices for an adequate resolution of the Langmuir spectral feature and its vicinity. It is convenient to express the simulation time in terms of the electron plasma period $\tau_{pe} = 2\pi/\omega_{pe}$. Figure 6 displays the fluctuation power spectra as obtained by simulations with $N_e^s = 5000$, $r_0 = 1.0\ \lambda_{De}$ and varying $t_{sim}$ values. We observe the following: (i) It is evident that $t_{sim} < 80\tau_{pe}$ leads to noticeably distorted spectra. The simulation results in the vicinity of the Langmuir mode have essentially converged for $t_{sim} \geqslant 80\tau_{pe}$ and only small improvements can be gained by performing longer simulations. (ii) As expected, it is demonstrated that longer simulation times allow us to capture physics relevant for lower frequencies. It is worth noting that the simulations correctly reproduce the part of the spectrum that arises from the ion dynamics. (iii) At very high frequencies the simulated spectra reach a lower bound.

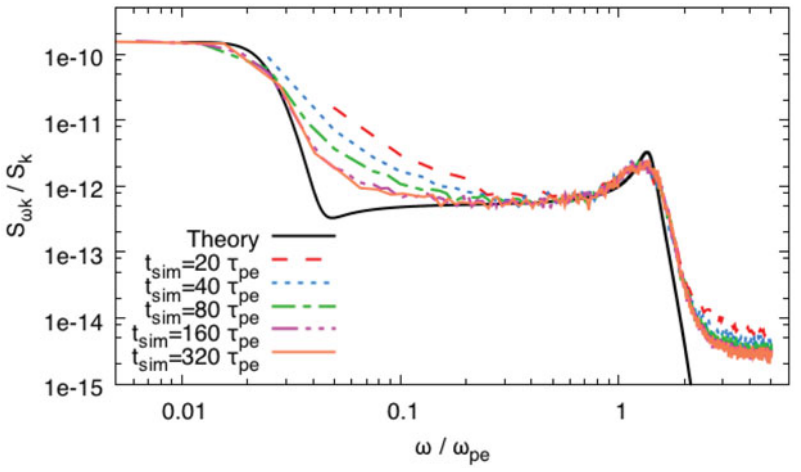


FIGURE 6. Spectral densities of electron density fluctuations for $k = 2 \times 10^4$ m$^{-1}$, $r_0 = 1.0\ \lambda_{De}$, $N_e^s = 5000$ and varying values of the simulation duration $t_{sim}$.

The intensity of the background noise is determined by the time step, with shorter time steps resulting in lower background.

*The number of simulated particles*. An increase of the particle number leads to a decrease of the particle weight $w$ and implies that the simulated system approaches the real system also as far as collisional aspects are concerned. Therefore, the effect of the simulated particle number on the numerical power spectra has been investigated. Figure 4(*b*) shows results for $r_0 = 1.0\ \lambda_{De}$. Increasing the number of particles leads to an almost linear improvement of the Langmuir peak height, whereas the peak width is almost unaffected.

*The numerical cutoff*. We shall explore the role of the cutoff radius $r_0$ on the numerical power spectra. Linear fluctuation theory (see § 2) neglects large amplitude fluctuations induced by collisions that occur at distances shorter than the Coulomb radius. As discussed in § 4, the simulated Coulomb radius depends on the number of simulated particles through the particle weight. This suggests that the numerical cutoff should always be chosen to be larger than $r_C^s$. Figure 7(*a*), where results for $N_e^s = 25\,000$ – corresponding to $r_C^s = 0.3\ \lambda_{De}$ – and different values for $r_0$ are compared to the theoretical spectrum for $k = 10^4$ m$^{-1}$, supports this conclusion. The agreement with the theoretical spectra improves by reducing $r_0$, but only as long as the condition $r_0 > r_C^s$ is satisfied. For cutoff values $r_0 < r_C^s$, large angle collisions are included in the simulation that appreciably distort the numerical power spectrum. Therefore, the optimal value is close to $r_0 = r_C^s$. Figure 7(*b*) compares results obtained with different simulated particle numbers and different cutoff radii $r_0$. We notice that it is this parameter that mainly affects the width of the simulated peak.

## 6. Numerical results

Having explored the dependence on the main simulation parameters, we shall now present numerical results obtained with the most computationally demanding simulation performed. The time step is $dt = 0.01\ \tau_{pe}$ and the numerical cutoff is $r_0 = 0.1\ \lambda_{De}$. The simulation domain is a cubic box of dimension $L = 26.7\ \lambda_{De}$, and $N_e^s = 25\,000$ is employed. The latter parameters lead to a particle weight $w \simeq 10^6$. As a consequence:

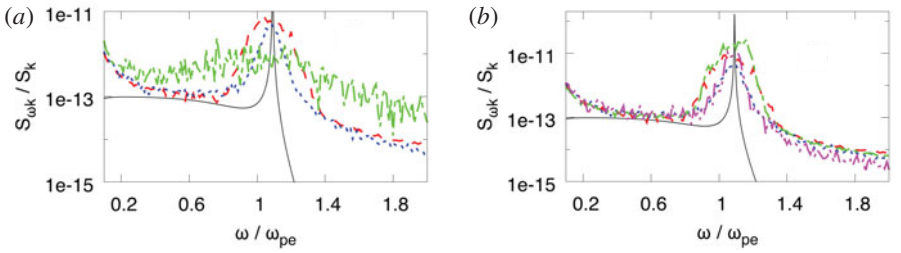


FIGURE 7. Spectral densities of electron density fluctuations for $k = 10^4$ m$^{-1}$. The cutoff radius, $r_0$, is expressed in $\lambda_{De}$ units. (*a*) $N_e^s = 25\,000$. Black: theory, red: $r_0 = 1.0$, blue: $r_0 = 0.1$, green: $r_0 = 0.01$. (*b*) Results obtained with different simulated particle numbers and different cutoff radii. Black: theory, red: $N_e^s = 25\,000$, $r_0 = 1.0$, blue: $N_e^s = 25\,000$, $r_0 = 0.1$, green: $N_e^s = 75\,000$, $r_0 = 1.0$, magenta: $N_e^s = 50\,000$, $r_0 = 0.1$.

(i) The electron–ion collision frequency is $\bar{\nu}_{ei}^s \simeq 2.2 \times 10^{10}$ s$^{-1}$ $\simeq 0.04\omega_{pe}$, which implies that the excess collisionality of the simulated system cannot shift the position of the Langmuir mode but can broaden the width of the spectral density maximum for wavenumbers that correspond to weak Landau damping.

(ii) The coupling parameter is $\Gamma^s \simeq 0.1$ and the normalized screening parameter is $\kappa^s \simeq 0.8$, which implies that the simulated system is non-ideal but still weakly coupled (Hamaguchi, Farouki & Dubin 1996), the excess coupling cannot displace the Langmuir mode but it can influence the width of the spectral density maximum.

(iii) The Coulomb radius is $r_C^s \simeq 1.43 \times 10^{-6}$ m $\simeq 0.06\lambda_{De}$, $r_0 > r_C^s$ ensures that large angle scattering is removed from the simulations but it also implies that short distance binary collisions are neglected, which is again most likely to affect the width of the spectral density maximum.

The power spectra for different wavelengths are presented in figure 8. The agreement with the theoretical results is excellent up to $k\lambda_{De} \gtrsim 0.5$ for the chosen simulation parameters that imply a cutoff radius $r_0 = 0.1\,\lambda_{De}$, i.e. six orders of magnitude larger than the Coulomb radius of the real system. At those wavelengths, the effect of Landau damping overcomes the combined effect of excess collisionality and coupling. Note also how the agreement extends well below the electron plasma frequency, down to 0.01 $\omega_{pe}$ where the ion dynamics is starting to contribute. At the smaller wavenumber, the excess collisionality of the MD simulation produces noticeable broadening of the Langmuir peak. The agreement can be extended towards the long wavelength limit, $k\lambda_{De} \ll 1$, (where the Langmuir peak becomes a delta function) by increasing the number of simulated particles, although at a high computational cost.

## 7. Conclusions

A numerical code based on classical molecular dynamics has been employed for the computation of the spectral densities of fluctuations of ideal collisionless plasmas aiming to verify limits and performances of such calculations in the light of possible generalizations, e.g. collisional or non-ideal plasmas. The implementation of a particle weight (to reduce the computational cost) in combination with the introduction of a short-range cutoff radius in binary interactions (to exclude spurious large angle

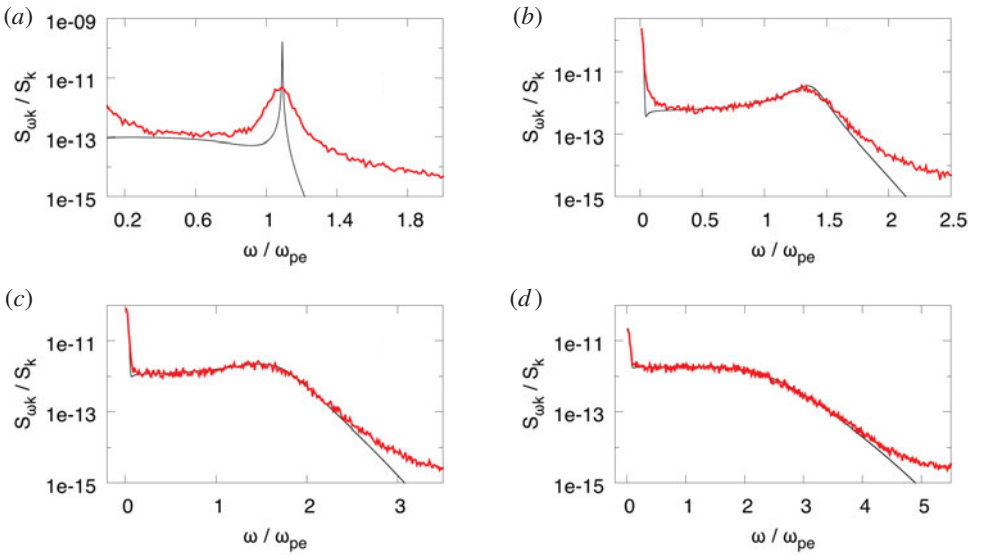


FIGURE 8. Spectral densities of electron density fluctuations, simulations (red) and theory (black), for different wavenumbers; (*a*) $k = 10^4$ m$^{-1}$; (*b*) $k = 2.0 \times 10^4$ m$^{-1}$; (*c*) $k = 3.0 \times 10^4$ m$^{-1}$; (*d*) $k = 5.0 \times 10^4$ m$^{-1}$. The simulation parameters are detailed in the text.

scattering) has led to the reproduction of the theoretical spectra with reasonable accuracy within contemporary computing capabilities. The scaling employed in the simulated system preserves the collective properties of the real system but not its collisional properties. The additional collisionality and coupling lead to deviations from the theory, which are more prominent for small wavenumbers that are characterized by weak collisionless damping. Even in this case, the position of the spectral maximum, that depends on the collective properties, is well reproduced and the deviations concern the peak height and mainly the full width at half-maximum. On the other hand, for large wavenumbers the agreement is very strong. Since the differences between the simulated and real system are manifold (collisionality, coupling, short-range collisions), it has not been possible to extrapolate on the computing resources that would be necessary for complete convergence with theory. However, the observed improvement with increasing particle number is encouraging.

**Acknowledgements**

S.L. and A.P. acknowledge the PON project 'Apulia Space' for financial support. P.T. and S.R. would like to acknowledge the financial support of the Swedish Research Council. We acknowledge the CINECA award under the ISCRA initiative, for the availability of GALILEO high performance computing resources and support for the projects: HP10CVMSRO, HP10CMOJLH. We acknowledge PRACE (Project 2010PA3211) for awarding us access to resources: FERMI based in Italy at CINECA, HAZEL HEN based in Germany at the High Performance Computing Centre (HLRS), JUQUEEN based in Germany at the Jülich Research Centre (FZJ) and SuperMUC based in Germany at Leibniz Supercomputing Centre (LRZ).

## REFERENCES


ABDUL, R. F. & MACE, R. L. 2015 One-dimensional particle-in-cell simulations of electrostatic Bernstein waves in plasmas with kappa velocity distributions. *Phys. Plasmas* **22**, 102107.

AKHIEZER, A. I., AKHIEZER, I. A., POLOVIN, R. V., SITENKO, A. G. & STEPANOV, K. N. 1975 *Plasma Electrodynamics Volume 2: Non-Linear Theory and Fluctuations*. Pergamon Press.

ALEXANDROV, A. F., BOGDANKEVICH, L. S. & RUKHADZE, A. A. 1984 *Principles of Plasma Electrodynamics*. Springer.

DHARUMAN, G., STANTON, L. G., GOSLI, J. N. & MURILLO, M. S. 2017 A generalized Ewald decomposition for screened Coulomb interactions. *J. Chem. Phys.* **146**, 0241112.

DONKO, Z., KALMAN, G. J. & HARTMANN, P. 2008 Dynamical correlations and collective excitations of Yukawa liquids. *J. Phys.* **20** (41), 413101.

FRIGO, M. & JOHNSON, S. G. 2005 The design and implementation of FFTW3. *Proc. IEEE* **93** (2), 216–231.

HAMAGUCHI, S., FAROUKI, R. T. & DUBIN, D. H. E. 1996 Phase diagram of Yukawa systems near the one component plasma limit revisited. *J. Chem. Phys.* **105**, 7641.

KLIMONTOVICH, YU. L. 1967 *The Statistical Theory of Non-equilibrium Processes in a Plasma*. Pergamon Press.

KLIMONTOVICH, Y. L., WILHELMSSON, H., YAKIMENKO, I. P. & ZAGORODNY, A. G. 1989 Statistical theory of plasma-molecular systems. *Phys. Rep.* **175** (5–6), 263.

KOLBERG, U., SCHLICKEISER, R. & YOON, P. H. 2017 Velocity fluctuations driven by the damped aperiodic mode in the intergalactic medium. *Astrophys. J.* **844**, 124.

LOPEZ, R. A. & YOON, P. H. 2017 Simulation of electromagnetic fluctuations in thermal magnetized plasma. *Plasma Phys. Control. Fusion* **59**, 115003.

MEIERBACHTOL, C. S., SVYATSKIY, D., DELZANNO, G. L., VERNON, L. J. & MOULTON, J. D. 2017 An electrostatic Particle-In-Cell code on multi-block structured meshes. *J. Comput. Phys.* **350**, 796–823.

NOSÉ, S. 1984 A unified formulation of the constant temperature molecular dynamics methods. *J. Chem. Phys.* **81**, 511.

SCHLICKEISER, R. 2012 Cosmic magnetization: from spontaneously emitted aperiodic turbulent to ordered equipartition fields. *Phys. Rev. Lett.* **109**, 261101.

SHEFFIELD, J. 1975 *Plasma Scattering of Electromagnetic Radiation*. Academic Press.

SITENKO, A. G. & GURIN, A. A. 1966 Effect of particle collisions on plasma fluctuations. *Sov. Phys. JETP* **22** (5), 1089.

TOLIAS, P. & RATYNSKAIA, S. 2013 Scattering of radiation in collisionless dusty plasmas. *Phys. Plasmas* **20**, 043706.

TOLIAS, P., RATYNSKAIA, S. & DE ANGELIS, U. 2011 Kinetic models of partially ionized complex plasmas in the low frequency regime. *Phys. Plasmas* **18**, 073705.

TOLIAS, P., RATYNSKAIA, S. & DE ANGELIS, U. 2012 Spectra of ion density and potential fluctuations in weakly ionized plasmas in the presence of dust grains. *Phys. Rev.* E **85**, 026408.

TOLIAS, P., RATYNSKAIA, S., PANARESE, A., LONGO, S. & DE ANGELIS, U. 2015 Natural fluctuations in un-magnetized and magnetized plasmas. *J. Plasma Phys.* **81** (3), 905810314.

TSYTOVICH, V. N. & DE ANGELIS, U. 1999 Kinetic theory of dusty plasmas. I. General approach. *Phys. Plasmas* **6** (4), 1093.

YOON, P. H. & LOPEZ, R. A. 2017 Spontaneous emission of electromagnetic fluctuations in magnetized plasmas. *Phys. Plasmas* **24**, 0221117.

YOON, P. H., SCHLICKEISER, R. & KOLBERG, U. 2014 Thermal fluctuation levels of magnetic and electric fields in unmagnetized plasma: the rigorous relativistic kinetic theory. *Phys. Plasmas* **21**, 032109.